Mechanisms and potential immune tradeoffs of accelerated coral growth induced by microfragmentation

Louis Schlecker[1], Christopher Page[2], Mikhail Matz[3] and Rachel M. Wright[1,3]

[1] Smith College, Northampton, Massachusetts, United States
[2] Mote Marine Laboratory, Summerland Key, Florida, USA
[3] University of Texas at Austin, Austin, Texas, United States

ABSTRACT

Microfragmentation is the act of cutting corals into small pieces (~1 cm^2) to accelerate the growth rates of corals relative to growth rates observed when maintaining larger-sized fragments. This rapid tissue and skeletal expansion technique offers great potential for supporting reef restoration, yet the biological processes and tradeoffs involved in microfragmentation-mediated accelerated growth are not well understood. Here we compared growth rates across a range of successively smaller fragment sizes in multiple genets of reef-building corals, *Orbicella faveolata* and *Montastraea cavernosa*. Our results confirm prior findings that smaller initial sizes confer accelerated growth after four months of recovery in a raceway. *O. faveolata* transcript levels associated with growth rate include genes encoding carbonic anhydrase and glutamic acid-rich proteins, which have been previously implicated in coral biomineralization, as well as a number of unannotated transcripts that warrant further characterization. Innate immunity enzyme activity assays and gene expression results suggest a potential tradeoff between growth rate after microfragmentation and immune investment. Microfragmentation-based restoration practices have had great success on Caribbean reefs, despite widespread mortality among wild corals due to infectious diseases. Future studies should continue to examine potential immune tradeoffs throughout the microfragmentation recovery period that may affect growout survival and disease transmission after outplanting.

Subjects Bioinformatics, Conservation Biology, Genomics, Marine Biology, Climate Change Biology

Keywords Microfragmentation, Coral immunity, Growth and immunity, Immunity tradeoffs, *Orbicella faveolata*, *Montastraea cavernosa*, Innate immunity, Reef restoration, Coral genomics, Outplanting

Submitted 17 September 2021
Accepted 2 March 2022
Published 29 March 2022

Corresponding author
Rachel M. Wright,
rwright@smith.edu

Academic editor
Anastazia Banaszak

Additional Information and Declarations can be found on page 19

DOI **10.7717/peerj.13158**

INTRODUCTION

Reefs occupy less than 1% of the ocean area, but the physical structures produced by calcifying reef corals support roughly 34% of the ocean's biodiversity (*Reaka-Kudla, 2001*). A variety of environmental factors threaten this biodiversity as coral ecosystems rapidly decline (*Hoegh-Guldberg et al., 2007*; *Sully et al., 2019*; *Dietzel et al., 2020*). The Caribbean has experienced 50–80% reductions in coral cover in the last few decades due to

increasingly frequent and intense bleaching events, hurricanes, and disease outbreaks (*Aronson & Precht, 2001*; *Gardner et al., 2005*; *Hoegh-Guldberg et al., 2007*; *Miller et al., 2009*, *Sully et al., 2019*). Coral disease was rarely identified before 1980, but has become more prevalent with rising temperatures (*Bruno et al., 2007*; *Harvell et al., 2007*). There are now over 40 recognized coral diseases affecting roughly 200 coral species in over 75 countries (*Bruckner, 2016*). Some areas of Florida's reefs have been reduced to less than 3% of their previously recorded population densities in part due to disease, which is a consequence of complex interactions between biotic (e.g., pathogen abundance) and abiotic (e.g., temperature) factors (*Randall et al., 2014*; *Precht et al., 2016*). However, some reports suggest these declines may have begun before disease outbreaks became prominent (*Cramer et al., 2020*). Stony Coral Tissue Loss Disease (SCTLD) was first reported off the southeast coast of Florida in 2014 after a major bleaching event and has since spread quickly throughout the Caribbean (*Weil et al., 2019*), further contributing to Caribbean coral loss (*Meiling et al., 2021*). The etiology of SCTLD is currently unknown, though some bacterial taxa are strongly associated with pathogenesis (*Rosales et al., 2020*; *Landsberg et al., 2020*), and multiple studies have shown that an interventive antibiotic treatment can slow lesion progression (*Aeby et al., 2019*; *Neely et al., 2020*; *Shilling, Combs & Voss, 2021*). These declines in coral cover demonstrate that active restoration efforts are increasingly necessary to help prevent the loss of coral ecosystems in the Caribbean, though gaps in restoration science can limit the effectiveness of management practices (*Boström-Einarsson et al., 2020*).

One coral restoration technique is microfragmentation: a process in which corals are divided into very small pieces (usually 1–3 cm^2) that then grow rapidly to generate coral biomass (*Forsman et al., 2015*; *Page, Muller & Vaughan, 2018*). Coral fragments can be directly outplanted or transferred to a land-based or *in situ* nursery to grow for 6–12 months before being outplanted to a recipient reef (*Page, Muller & Vaughan, 2018*). Microfragmentation offers clear benefits for quickly generating coral biomass, but much remains unknown about the biological processes and potential consequences of this rapid growth. Previous work demonstrates that variation in growth rate among calcifying corals can be a poor predictor of overall fitness (*Edmunds, 2017*). Like all living organisms, a coral's energetic budget simultaneously supports all aspects of growth and homeostasis (*Lesser, 2013*), including immune activity to prevent disease (*Palmer, 2018*) and lesion repair to heal physical wounds (*Denis et al., 2011*). Corals experiencing environmental challenges on today's reefs will not survive if they cannot sustain rapid growth along with robust responses to biotic and abiotic threats.

Corals rely on innate immunity to ward off infection by invading pathogens (*Palmer & Traylor-Knowles, 2012*). Key players of these immune activities include phenoloxidase, an enzyme involved in the melanin synthesis pathway (*Mydlarz & Palmer, 2011*), and antioxidant enzymes catalase and peroxidase (*Palmer et al., 2011*). Melanization contributes to coral disease resistance and clearance by concentrating cytotoxic melanin around invading pathogens and damaged tissue (*González-Santoyo & Córdoba-Aguilar, 2012*). The melanization process and other host responses to pathogens produce reactive oxygen species as byproducts that provide additional antimicrobial defenses (*Cerenius, Lee*

& Söderhäll, 2008), but can potentially damage the host's healthy tissue (Sadd & Siva-Jothy, 2006). Thus, antioxidant enzymes such as peroxidase and catalase are also integral to immune activity (Mydlarz, McGinty & Harvell, 2010). Coral fluorescent proteins may also provide peroxide scavenging properties that aid immunity (Palmer, Modi & Mydlarz, 2009).

Gene expression analyses provide molecular insight to stress responses in corals. For example, peroxidase expression has been associated with coral responses to thermal stress and disease (Mydlarz & Harvell, 2007; Wright et al., 2017; Traylor-Knowles et al., 2021). Gene expression analyses have also highlighted the importance of other cellular mechanisms to manage disease, such as programmed cell death. *O. faveolata* and *M. cavernosa* upregulated apoptosis-related genes when exposed to SCTLD (Traylor-Knowles et al., 2021). Corals lack the adaptive immunity required to recognize specific pathogens from previous exposures, but they do possess receptors that recognize general pathogen-associated molecular patterns, such as Toll-Like Receptors (TLRs) (reviewed in Nie et al., 2018). TLRs have been characterized in *O. faveolata* (Williams et al., 2018) and were upregulated in *Acropora hyacinthus* affected with white syndromes (Wright et al., 2015). Antimicrobial peptides (AMPs) provide another innate immune mechanism to restrict bacterial infections by directly targeting bacterial cells and by initiating TLR immune pathways (Lee, Lee & Wong, 2019). Differential expression of AMPs in response to *Vibrio* challenge has been documented in the reef-building coral *Pocillopora damicornis* (Vidal-Dupiol et al., 2011). Lectins are another type of bioactive peptide that can recognize non-self molecular patterns to activate immune mechanisms in corals (Palmer & Traylor-Knowles, 2012). C-type lectin was downregulated in *O. faveolata* affected with White Plague Disease relative to healthy corals, suggesting a diminished capacity for affected corals to respond to bacterial infection (Daniels et al., 2015).

The cellular machinery driving calcification, immune defense, and tissue regeneration requires energetic investment. The present study implemented variable size fragmentation that induced different growth rates to study the biological underpinnings of and potential tradeoffs associated with rapid growth in reef-building corals *O. faveolata* and *M. cavernosa*. The association between innate immune enzyme levels and initial fragment size indicates the relationship between investment in growth and immunity. Transcriptomic analysis by initial fragment size (i.e., the extent of microfragmentation) and buoyant weight change identified genes associated with microfragmentation and calcification.

MATERIALS AND METHODS

Coral collection, microfragmentation, and growth

Large fragments (~140–370 cm^2) of five colonies from each species (*M. cavernosa* and *O. faveolata*) were collected from the NOAA Rescue Nursery in Key West, a repository for stony corals which were rescued from construction sites, in November 2015 under Florida Keys National Marine Sanctuary (FKNMS) permit FKNMS-2015-130. These large colonies were first processed on 10 Nov 2015 using a seawater-cooled tile saw (MK 101 Pro Series; MK Diamond Products Inc., Torrance, CA, USA) to remove the majority of the

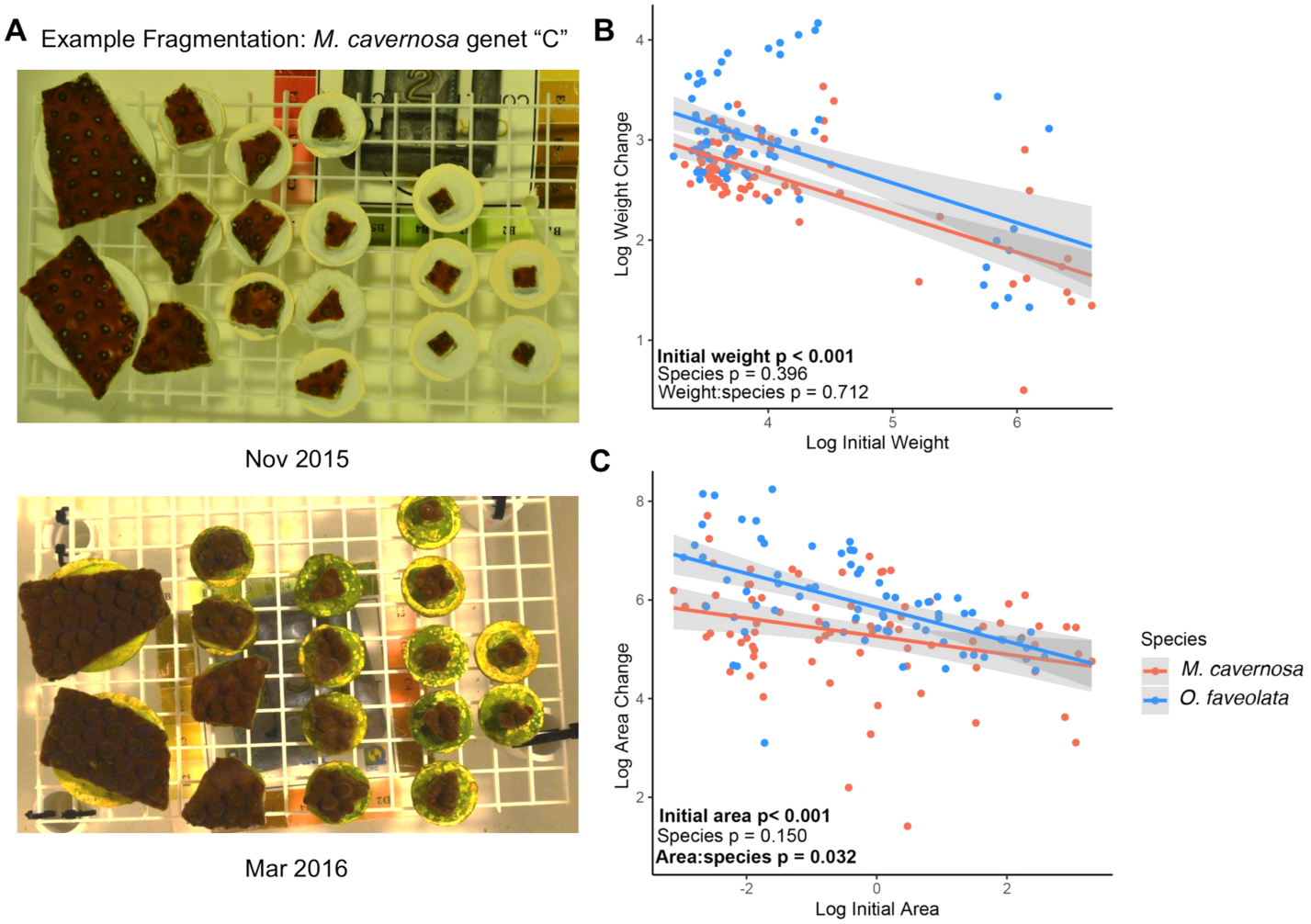

Figure 1 Smaller fragments grow faster. (A) Example photographs of coral fragments from a single *M. cavernosa* genet "C" taken in Nov 2015 (top) and after the 4-month recovery period in March 2016 (bottom). (B) Relationships between log-transformed initial weight and change in buoyant weight and log-transformed initial area and change in surface area (C) for *M. cavernosa* (red) and *O. faveolata* (blue). Each point represents an individual coral fragment (B and C). Shaded lines represent 95% confidence intervals for the linear regression between initial size and growth. *P*-values represent results from the MCMC model testing the individual effects of initial size and species, and the interaction between initial size and species. Significant values are in bold.
Full-size DOI: 10.7717/peerj.13158/fig-1

dead skeleton from the base of each colony. Colonies were then cut into a range of fragment sizes from about 0.1–10 cm^2 using a seawater cooled diamond band saw (C-40; Gryphon Corporation, Foothill Boulevard, CA, USA) and mounted to cement plugs using underwater epoxy (Allfix; Cir Cut Corporation, Philadelphia, PA, USA). Each fragment was photographed with a color and size standard (example in Fig. 1A) and weighed following the buoyant weight protocol (*Spencer Davies, 1989*). Surface areas were measured using ImageJ (*Schneider, Rasband & Eliceiri, 2012*).

Fragments were then placed in a 340 L raceway supplied with ~35 ppt seawater from a 24 m deep well. Seawater exiting the well was degassed of CO_2 and filtered mechanically using a sand filter and 100 µm pleated filter (Pentair Aquatic Ecosystems Inc., Apopka, FL, USA) to bring the pH to 7.7 before entering the raceway at a rate of

2.5 Lpm. The raceway was supplied with four 3 cm airstones (Sweetwater; Pentair Aquatic Ecosystems, Apopka, FL, USA) to further degas incoming seawater to a pH of 8.0 and to provide circulation. Additionally, the raceway was housed under a metal canopy lined with 40% shade cloth, and later draped with an additional shade cloth at 14:00 to prevent over irradiance, such that the photosynthetically active radiation during the day ranged from ~60–700 µmol $m^{-2}s^{-2}$, peaking during midday (Model QMSS-E; Apogee Instruments Inc., Logan, UT, USA). Daily siphoning, grazing by the sea snail *Lithopoma tecta*, and periodic manual removal of long chain diatoms kept fragments free of invasive algae during the experiment. Fragments were photographed and weighed again on 12 March 2016 using the same measurement protocols as previously described. After weighing, a small (~1 cm^2) amount of tissue was preserved in ethanol for gene expression analysis. The remaining tissue was snap-frozen on dry ice and preserved at −80 °C for protein analysis.

We note that some surface areas of the largest fragments may be underestimated due to limitations in the photographic method used for measurements. Some of the larger fragments had grown over and down the side of the cement pucks, out of the field of view from the top-down photographs (example images in Fig. 1A). Thus, we focus on growth in terms of weight captured by the sensitive buoyant weight method, which represents skeletal growth that is deposited by living tissue, for the subsequent associations between growth and immune activity or gene expression.

Immune activity assays

Coral protein was extracted following previously described protocols (*Wright et al., 2017*). Briefly, coral tissue was removed using an airbrush and cold (4 °C) extraction buffer (100 mM Tris-HCl, pH 7.8, with 0.05 mM dithiothreitol). The resulting tissue slurries were homogenized by vortexing samples with a small amount of 1 mm glass beads (BioSpec, Bartlesville, OK, USA) for two minutes. The homogenized tissue slurry was centrifuged at 4 °C for 10 min at 3,200 g to separate coral and algal fractions. The coral protein supernatant (protein extraction) was removed and stored at −80 °C until use. Surface area determinations of airbrushed skeletons were made using the foil technique (*Marsh, 1970*). Briefly, aluminum foil was carefully trimmed along the area of the coral skeleton where tissue was removed. The weight of the trimmed foil was compared to a standard curve of known surface areas to estimate the surface area.

Total protein was assessed in triplicate using the RED660 protein assay (G Biosciences, St. Louis, MO, USA) with a bovine serum albumin standard curve. Sample absorbance, measured at 660 nm using a SpectraMax plate reader (Molecular Devices), was compared to the standard curve and normalized to tissue surface area and slurry volume to account for dilution with extraction buffer.

Immune enzyme activities were measured in triplicate as previously described (*Wright et al., 2017*). Active phenoloxidase (PO) activity was measured by mixing 20 µL of sodium phosphate buffer (50 mM, pH 7.0), 25 µL of sterile water, and 20 µL of protein extract. Dopamine (30 µL, 10 mM) was added as substrate and absorbance at 490 nm was measured every 30 s for 15 min. Change in absorbance was calculated during the linear

range of the curve (1–3 min). Activity was expressed as the change in absorbance per mg of protein (ΔA490 · mg protein^{-1} · min^{-1}). Total phenoloxidase activity (PPO), including the inactive prophenoloxidase and active PO, was measured the same as PO except for the addition of 25 µL of trypsin (0.1 mg · mL^{-1}) in the reaction buffer to activate prophenoloxidase. Catalase (CAT) activity was measured by mixing 45 µL of sodium phosphate buffer (50 mM, pH 7.0), 75 µL of 25 mM H_2O_2, and 5 µL of protein extract. Samples were loaded on ultraviolet transparent plates (UltraCruz; Santa Cruz Biotechnology, Dallas, TX, USA) and absorbance at 240 nm was measured every 30 s for 15 min. Change in absorbance was calculated during the linear range of the curve (1–3 min). Activity was expressed as the change in hydrogen peroxide concentration per mg of protein (ΔH_2O_2 · mg protein^{-1} · min^{-1}). Peroxidase (POX) activity was measured by mixing 40 µL of sodium phosphate buffer (10 mM, pH 6.0), 25 µL of 10 mM guaiacol, and 10 µL of protein extract. Absorbance at 470 nm was measured every 30 s for 15 min. Change in absorbance was calculated during the linear range of the curve (1–3 min). Activity was expressed as the change in absorbance per mg of protein (ΔA470 · mg protein^{-1} · min^{-1}).

Tag-Seq library preparation, sequencing, and analysis

A small (<1cm^2) amount of tissue was removed from the growing edge of each coral fragment and immediately preserved in cold ethanol before transfer to −80 °C. The remaining coral tissue was preserved for protein analysis as previously described. RNA was isolated from each tissue sample using the RNAqueous Total RNA Isolation Kit (Invitrogen, Waltham, MA, USA). A total of 65 gene expression libraries, prepared following the TagSeq protocol (*Meyer, Aglyamova & Matz, 2011*), were of high enough quality for Illumina HiSeq 2500 sequencing (SRA: PRJNA764071). Reads were deduplicated, adapter sequences were trimmed, and low-quality reads (minimum quality score = 20; minimum percent bases above minimum quality score = 90%) were filtered using FASTX toolkit (*Hannon, 2010*). To determine dominant symbiont types for each species, we mapped TagSeq reads to a combined symbiont reference composed of transcriptomes from Symbiodiniaceae 'clades' A (Genus *Symbiodinium*) and B (Genus *Breviolum*) (*Bayer et al., 2012*) and 'clades' C (Genus *Cladocopium*) and D (Genus *Durusdinium*) (*Ladner, Barshis & Palumbi, 2012*) using a custom perl script 'zooxtype.pl'. Custom scripts for read deduplication and identifying Symbiodiniaceae genera are hosted within the 2bRAD GitHub repository (https://github.com/z0on/tag-based_RNAseq).

Trimmed TagSeq reads from *M. cavernosa* samples were mapped to a holobiont reference consisting of the *M. cavernosa* (Data & Code-Matz Lab), *Cladocopium goreaui* (*ReFuGe 2020 Consortium, 2015*), and *Durusdinium* genomes (*Shoguchi et al., 2021*) using Bowtie 2 (*Langmead & Salzberg, 2012*). Trimmed TagSeq reads from *O. faveolata* samples were mapped to a holobiont reference consisting of the *O. faveolata* (*Prada et al., 2016*) and *Durusdinium* genomes (*Shoguchi et al., 2021*). Reads were converted to counts representing the number of independent observations of a transcript over all isoforms for each gene. Significantly differentially expressed genes were characterized using NCBI BLAST (*Altschul et al., 1990*). Genes that returned no significant BLAST hit

were characterized using NCBI Conserved Domain Database (*Lu et al., 2020*) to predict functional protein domains.

Genes with a mean count of less than three across all samples were removed from the analysis, leaving 7889 genes for *M. cavernosa* and 9979 genes for *O. faveolata*. Read counts from technical replicates (libraries prepared from separate RNA extractions of the same coral fragment) were pooled before differential gene expression analysis.

Genotyping was performed with ANGSD v0.930 (*Korneliussen, Albrechtsen & Nielsen, 2014*) using coral reads mapped to their respective genomes as previously described. Sites were filtered to retain loci with a mapping quality ≥25 and minor allele frequency ≥0.05. Samples identified as clones in highly similar clusters based on distances among known clones (distance < 0.2) were re-identified as a single genet.

Statistics

All statistical analyses were performed in R version 4.0.2 (*RStudio Team, 2020*). Growth was estimated as the percent change in buoyant weight ($Weight_{Final} - Weight_{Initial}/Weight_{Initial} * 100$) and as the percent increase in area ($Area_{Final} - Area_{Initial}/Area_{Initial} * 100$). We also estimated growth using the power of an exponential process, $\log_2$(final size/initial size), which gave the same results as percent growth estimates. Associations between growth and initial size were analyzed using Bayesian generalized linear mixed models implemented in MCMCglmm package in R (*Hadfield, 2010*) with the interaction between initial size and species as fixed factors and genet as a random effect.

Activities of CAT, POX, PO, and PPO were normalized to the total protein concentration, log-transformed, and compared among initial sizes using MCMCglmm. We used initial size as our predictor variable to address our biological objective to determine the relationship between immune parameters and the extent of microfragmentation (*i.e.*, initial fragment size). Log-transformation was chosen based on diagnostic plots of a linear model with species, genet, and initial fragment size as factors. The MCMC model included the interaction between initial size and species as fixed effects and genet as a random effect. Additionally, we conducted a binned analysis using categorical assignments for initial size as "small" (≤mean initial weight) or "big" (>mean initial weight).

Gene expression sample outliers were detected using arrayQualityMetrics (*Kauffmann, Gentleman & Huber, 2009*). Differentially expressed genes (DEGs) were identified using DESeq2 (*Love, Huber & Anders, 2014*). Wald tests were performed to compare continuous growth phenotypes using the models 'count ~ genet + initial weight + weight change' where genet was a factor representing the colony from which the fragment was made and weight values were continuous measurements that were centered and scaled per DESeq2 recommendations for continuous predictor variables to improve generalized linear model convergence. A total of 27 *M. cavernosa* and 25 *O. faveolata samples* remained after combining technical replicates and outlier detection. The DESeq2 models were run independently for each species. Count data was transformed using the variance stabilizing transformation. We reported Wald statistics (log fold change/standard error) to represent the magnitude of expression difference per unit change of continuous variables. We repeated DESeq2 gene expression analysis using binned categories of

initial size and growth rate as previously described. False-discovery rate (FDR) p-values were adjusted using the Benjamini–Hochberg procedure (*Benjamini & Hochberg, 1995*). Gene expression heatmaps were generated using pheatmap (*Kolde, 2019*) and gene ontology enrichment was performed based on log-fold change values using GO-MWU (*Wright et al., 2015*). Permutational analysis of variance testing on Manhattan dissimilarity matrices (ADONIS) was performed using vegan (*Dixon, 2003*) to assess overall transcriptomic differences across samples. All analytical scripts and data files are available on GitHub (https://github.com/rachelwright8/Microfrag_Growth_Immunity_TagSeq).

A weighted gene correlation network analysis (WGCNA, *Langfelder & Horvath, 2008*) was used to correlate expression values for groups of co-regulated genes with traits. Genes with mean counts >3 were used to construct a signed network. A sample network was constructed to identify outlying samples with a standardized connectivity score of less than −2.5. A signed gene co-expression network was constructed with a soft threshold power of 12. Groups of co-regulated genes (modules) with a Pearson correlation coefficient 0.3 or higher were merged. GO enrichment for each module was performed as previously described, with the exception of using per-gene module membership values (kME) instead of log-fold change values.

RESULTS

Associations between growth and initial fragment size

Growth was monitored for 78 *M. cavernosa* and 74 *O. faveolata* microfragments as surface area expansion and as changes in buoyant weight, which included the weight of the cement plug. The mean ± SD values for initial area and weight across all *M. cavernosa* fragments were 1.72 ± 2.36 cm^2 and 22.8 ± 21.8 g, respectively. The mean ± SD values for initial area and weight across all *O. faveolata* fragments were 1.37 ± 1.46 cm^2 and 19.9 ± 16.7 g, respectively. After four months of growth, we observed a negative association between growth and initial fragment surface area (posterior mean = −0.17, $p < 0.001$) and between growth and buoyant weight (posterior mean = −0.30, $p < 0.001$) (Figs. 1B and 1C). There were no significant differences in mean growth between species. There was a significant interaction between species and surface area growth where *M. cavernosa* fragments displayed a less pronounced effect of microfragmentation on surface area growth than fragments of *O. faveolata* (posterior mean = −0.18; $p = 0.032$; Fig. 1C).

Plotting untransformed percent area increase for each fragment based on its initial size illustrates the range of microfragmentation-mediated growth effects (Fig. S1). We observed high variance in area increase below ~1 cm^2 ranging from tissue loss (−11%) to over 300% increase.

Immune activity analyses

We obtained enough tissue with measurable levels of protein to conduct the immune activity assays from 47 *M. cavernosa* and 49 *O. faveolata* fragments (Figs. 2A–2D). We observed positive associations between initial fragment size and rates of PO (posterior mean = 1.74; $p = 0.012$), PPO (posterior mean = 2.55; $p = 0.006$), and CAT (posterior mean = 2.70; $p < 0.001$) activities. Only POX activity was not significantly associated with

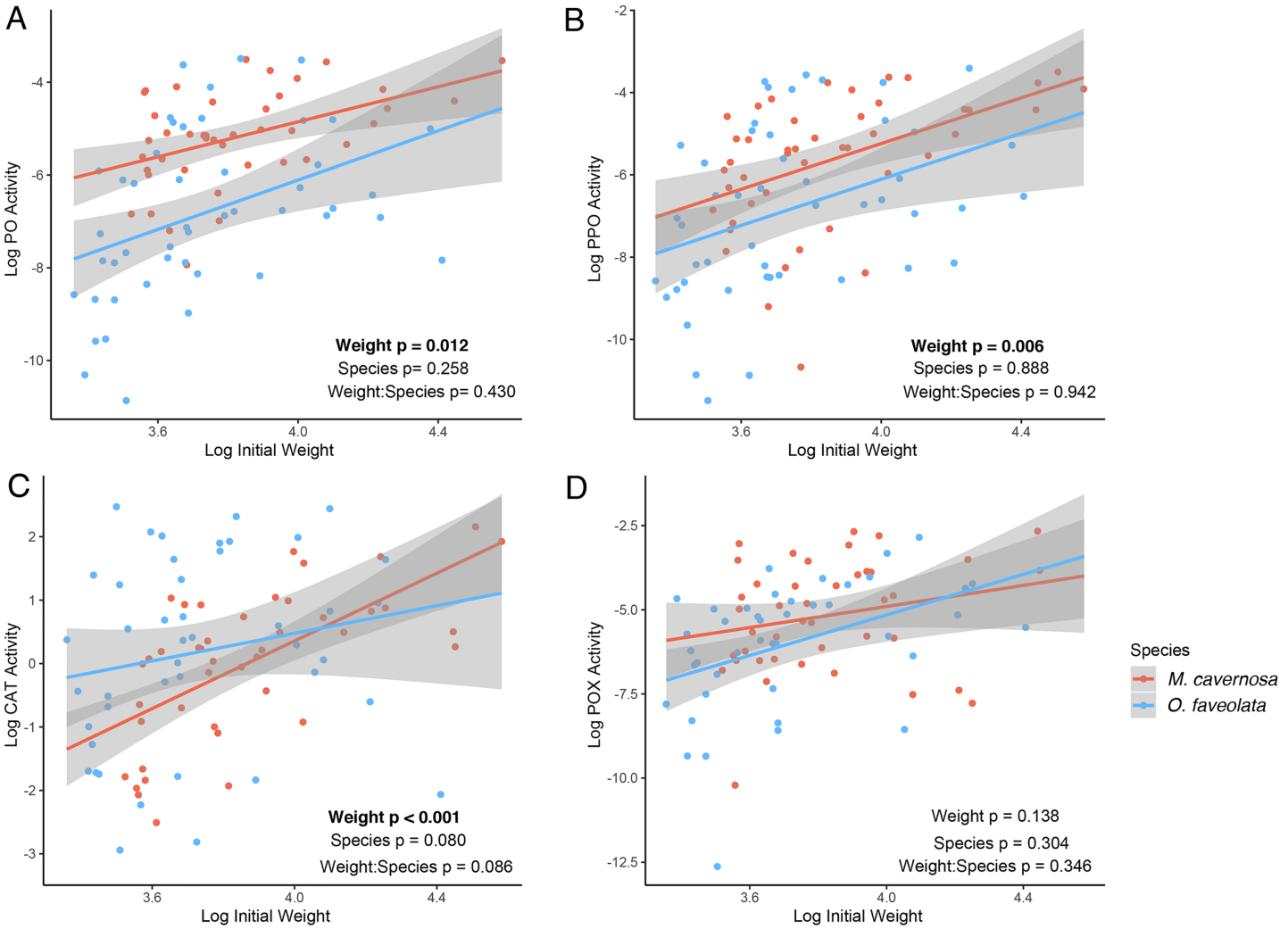

Figure 2 Associations between log-transformed initial weight and log-transformed immune activities for active phenoloxidase (A), total phenoloxidase potential (B), catalase (C), and peroxidase (D) in *M. cavernosa* (red) and *O. faveolata* (blue). Each point represents an individual coral fragment. Shaded lines represent 95% confidence intervals for the linear regression between initial size and growth. *P*-values represent results from the MCMC model testing the individual effects of and interaction between weight and species. Significant terms are indicated in bold.
Full-size DOI: 10.7717/peerj.13158/fig-2

coral size (posterior mean = 1.70; $p = 0.138$). There were no significant differences in immune activities between species. The binned analysis compared immune activities between fragments categorized as "big" (>mean initial weight, $N = 36$, mean ± SD = 17.5 ± 2.6 g) or "small" (≤mean initial weight, $N = 60$, mean ± SD = 12.3 ± 1.0 g). The binned analysis recapitulates the continuous analysis (Fig. S2). Larger fragments had higher PO (posterior mean = 0.97, $p = 0.012$), PPO (posterior mean = 1.37, $p = 0.010$), and CAT (posterior mean = 1.38, $p < 0.001$) activities than smaller fragments.

Identifying clones and dominant symbiont types

Genetic distance cluster analysis across *O. faveolata* genets revealed that two genets (previously named "V" and "X") were clones, which were renamed as genet "U" in

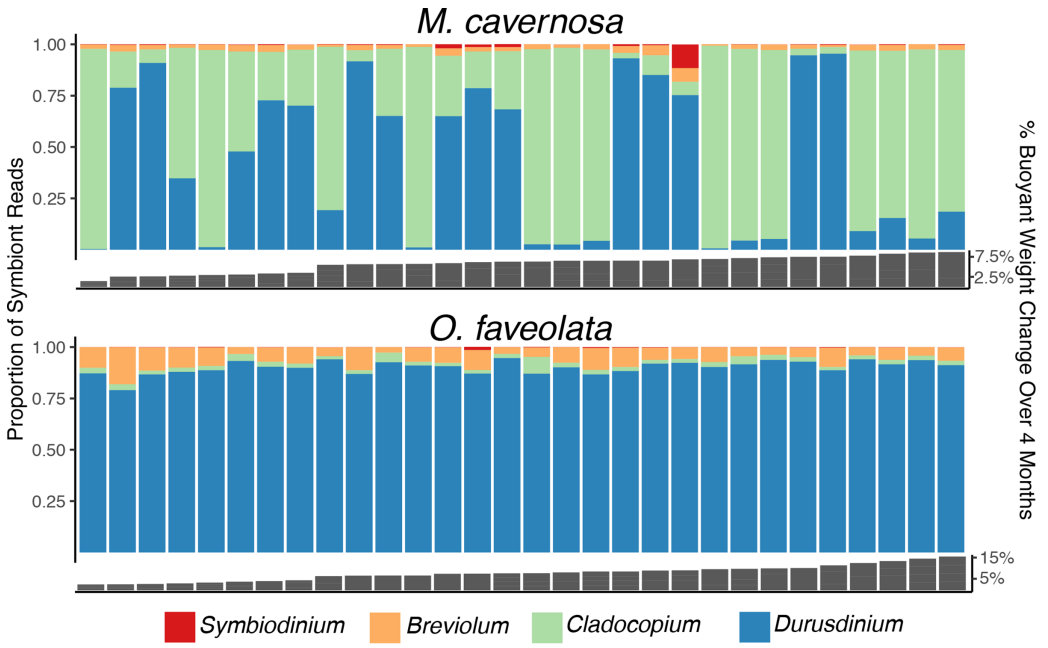

Figure 3 Determination of dominant algal symbiont types based on the proportion of reads mapping to each reference for *M. cavernosa* (top) and *O. faveolata* (bottom). Columns represent sequencing samples ordered by increasing buoyant weight percent increase (grey bars) from left to right. Colored bars represent the proportion of algal symbiont type reads according to the legend.

Full-size DOI: 10.7717/peerj.13158/fig-3

subsequent analysis (Fig. S3). Mapping *M. cavernosa* and *O. faveolata* reads to symbiont references determined that *M. cavernosa* hosted a mix of *Cladocopium* and *Durusdinium* while *O. faveolata* was dominated by *Durusdinium* (Fig. 3). We did not observe a significant association between growth (as percent surface area increase) and proportion *Durusdinium* reads in *M. cavernosa* samples (posterior mean = −50%, $p = 0.068$), or when measuring growth as percent change in buoyant weight (posterior mean = −0.84, $p = 0.422$) (Fig. S4).

M. cavernosa host expression profiles with respect to initial size and growth

The average *M. cavernosa* holobiont mapping efficiency was 85.2% with per-sample averages of 1.83×10^5 trimmed and filtered reads mapping to the host genome. In the coral host, initial size ($p = 0.014$, $r^2 = 0.07$) and genet ($p = 0.004$, $r^2 = 0.25$) explained the majority of the observed differences in gene expression profiles (Fig. S5A). Weight change was not significantly associated with variation in gene expression (Fig. S5B; $p = 0.416$). In the *M. cavernosa* holobiont analysis, only two host genes were significantly differentially expressed with respect to continuous growth rate at a threshold value of 0.1. These genes shared homology with transmembrane protein 86a (Mcavernosa16889) and guanylate binding protein (Mcavernosa20434). Transmembrane protein 86a expression had a positive association with growth (Wald stat = 4.35; FDR = 0.054) and guanylate binding

protein expression had a negative association with growth (Wald stat = −4.40; FDR = 0.054).

A binned gene expression analysis revealed 18 host genes that were significantly differentially expressed with respect to categorical initial fragment weight at FDR < 0.1 and 14 DEGs at FDR < 0.05 (Table S1). These genes include putative growth (*e.g.*, coadhesin) and immunity (*e.g.*, tachylectin-2) genes (Fig. S6). None of these 18 genes overlapped with the two DEGs identified using the continuous growth analysis.

We identified 28 significantly enriched (adjusted *p*-value < 0.1) gene ontology (GO) terms based on log-fold change values based on continuous weight change in the *M. cavernosa* host (Table S2). These enriched categories include terms related to protein synthesis and antioxidant responses. We did not identify any enriched GO terms for the host based on initial fragment size, nor did we find any enriched GO terms in the algal symbiont.

Using binned categories for initial fragment size and growth, we found four GO terms enriched with genes associated with initial fragment size and one GO term enriched with genes associated with growth (obsolete mitochondrial membrane part, delta rank = 444) (Table S2). The enriched terms regarding fragment size contained establishment of protein localization to membrane (delta rank = 468), ribosome (delta rank = 351), obsolete cytosolic part (delta rank = 385), and structural constituent of ribosome (delta rank = 417).

Several WGCNA modules represent potential expression tradeoffs between growth and immune metrics for *M. cavernosa* (Fig. 4). The green and violet modules were significantly positively associated with buoyant weight change and negatively correlated with immune parameters. The green module was enriched with genes related to structural constituents of ribosomes and mitotic cell cycle (Table S3), potentially reflecting genes associated with cellular growth. The dark magenta module was negatively associated with buoyant weight change and positively associated with immune parameters. This module had 52 significantly enriched GO terms, including "regulation of ossification," indicating the activity of genes that may be related to skeletal formation (*Scucchia et al., 2021*).

O. faveolata host expression profiles with respect to initial size and growth

The *O. faveolata* holobiont mapping efficiency was 81.8% with per-sample average reads of 2.06×10^5 mapping to the host genome. In the coral host, differences between genets ($p = 0.001$, $r^2 = 0.35$) explained the majority of the observed differences in gene expression profiles (Fig. S7A). Initial weight and weight change were not significantly associated with variation in gene expression (Fig. S7B; $p = 0.139$ and 0.162, respectively).

We identified 38 host *O. faveolata* genes significantly associated with continuous weight change over the 4-month recovery period at a *p*-value threshold of 0.1 (Fig. 5). Of these genes, seven were positively associated with growth rate and 31 were negatively associated with growth rate. A gene sharing sequence homology with glutamic acid-rich protein (LOC110061392) had higher expression in faster growing corals (Wald stat = 3.57,

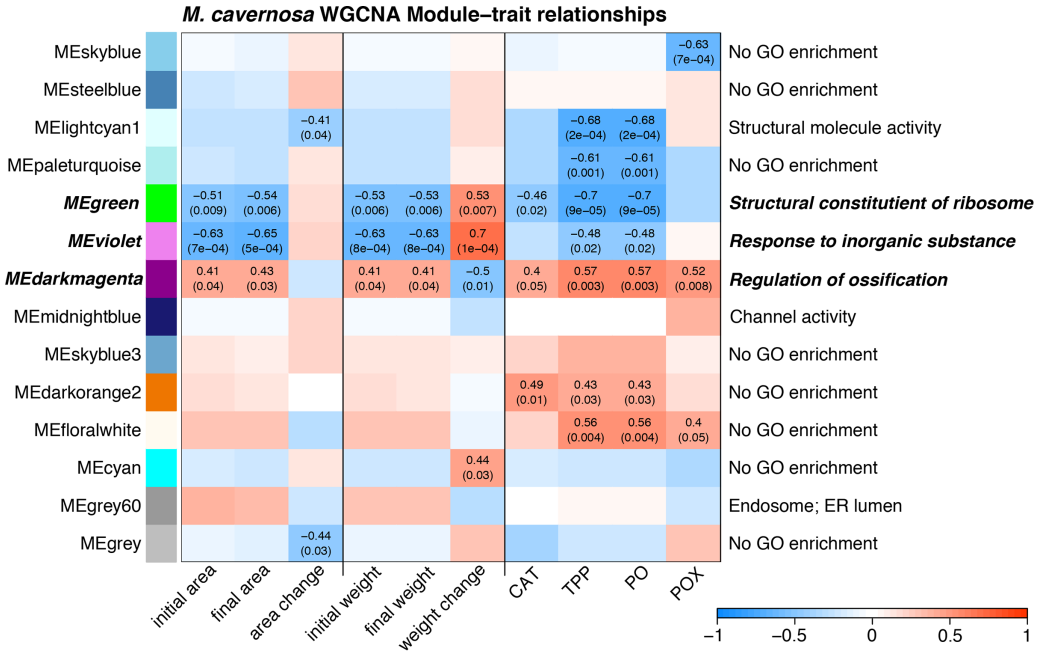

Figure 4 Module–trait relationship heatmap for *M. cavernosa*. The strength of the correlations between traits (terms indicated on along the x-axis) and gene coexpression modules (colored boxes along y-axis) are indicated by the intensity of color. Values within each cell indicate Pearson's correlation between the module eigengene and the trait and the *p*-value according to the correlation test for only significant correlations ($p < 0.05$). Terms along the right indicate a representative top enriched GO category for the module, if any. Modules in bold italic represent potential tradeoffs with opposite associations between growth and immune parameters. Full-size DOI: 10.7717/peerj.13158/fig-4

FDR = 0.096). Two transcripts with homology to carbonic anhydrases had lower expression in faster growing corals (LOC110047361 Wald stat = −3.76, FDR = 0.07 & LOC110047363 Wald stat = −5.94, FDR = 2.8e−5). Six immune-related genes were negatively associated with growth. These genes include integumentary mucin C.1 (LOC110061602; Wald stat = −3.71, FDR = 0.083), a component of coral mucus (*Jatkar et al., 2010*), and cathepsin L1-like (LOC110068187; Wald stat = −3.59, FDR = 0.096), which has been linked to many immunological responses (*Brown & Rodriguez-Lanetty, 2015*). A gene with homology to green fluorescent protein (GFP)-like chromoprotein cFP484 (LOC110044329) was also negatively associated with growth (Wald stat = −4.11; FDR = 0.054).

We identified 10 host *O. faveolata* genes significantly associated with categorical weight change (small *vs* large) at a p-value threshold of 0.1 (Table S1). Three of these DEGs overlap with the results of the continuous analysis: 9-divinyl ether synthase-like, an uncharacterized gene containing a deoxycytidylate deaminase domain, and an uncharacterized gene with no predicted protein domains.

We identified three enriched GO terms regarding fragment size and three enriched GO terms regarding growth using log-fold change values associated with *O. faveolata* host genes in the continuous growth analysis (Table S2). GO terms related to fragment size

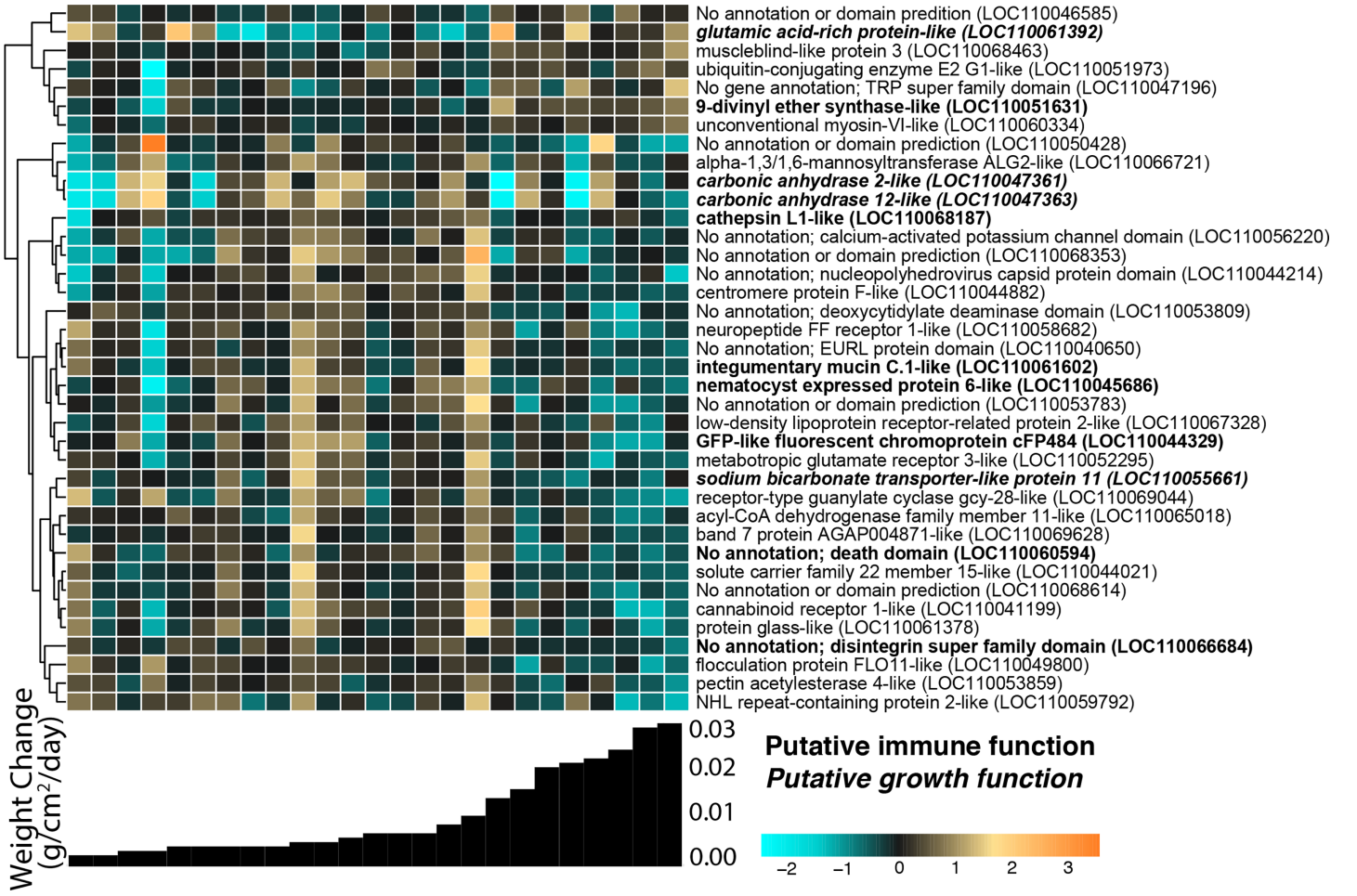

Figure 5 ***O. faveolata*** **gene expression differences across samples with different growth rates.** Rows are genes and columns are samples. The color scale indicates log2-fold change relative to the mean expression of each gene across all samples. Genes are hierarchically clustered based on Pearson's correlations of expression across samples. Bar graphs below each column represent the per-day growth rate as weight change per cm^2 over the 4-month recovery period for that sample. Genes with a putative immune function are highlighted in bold; genes with a putative growth function are bolded and italicized.
Full-size DOI: 10.7717/peerj.13158/fig-5

contained transmembrane signaling receptor activity (delta rank = −290), G protein-coupled receptor activity (delta rank = −349), and molecular transducer activity (delta rank = −221). GO terms relating to growth contained polytene chromosome (delta rank = 301), exocytic vesicle (delta rank = 309), and transmembrane signaling receptor activity (delta rank = −241). We found no enriched GO terms using binned categories for initial fragment size and growth.

Several WGCNA modules were correlated with immune activity in *O. faveolata*, but these results should be considered cautiously given the large number of gene expression samples for which we could not obtain enzymatic activity measurements for this species: only four *O. faveolata* gene expression samples had enzymatic measurements. However, we did have size and growth measurements for every sample. The light green module was significantly positively associated with buoyant weight change and enriched with terms related to reactive oxygen species metabolism (Fig. S8, Table S3). The green

yellow module was significantly positively associated with tissue growth as increased surface area and contained one enriched GO term: "muscle organ development".

Symbiont expression profiles with respect to initial size and growth

The average *M. cavernosa* holobiont mapping efficiency was 85.2% with trimmed and filtered reads with per-sample averages of 6.87×10^5 to *Cladocopium*, and 2.0×10^4 to *Durusdinium*. Variation in symbiont gene expression profiles were significantly associated with host genet in *Durusdinium* ($p = 0.002$) and marginally associated with weight change in *Cladocopium* ($p = 0.055$). Otherwise, symbiont gene expression was not significantly associated with any other host parameter (Fig. S9).

The *O. faveolata* holobiont mapping efficiency was 81.8% with per-sample average reads of 3.79×10^4 mapping to *Durusdinium*. Variation in symbiont gene expression was significantly associated with host genet ($p = 0.032$), but not initial weight or weight change over the 4-month recovery period ($p = 0.290$ and $p = 0.513$, respectively) (Fig. S10). We did not identify any significantly differentially expressed symbiont genes from the *O. faveolata* holobiont samples.

DISCUSSION

Microfragmentation confers accelerated coral growth with potential tradeoffs

The growth patterns in this study confirms what previous studies (*Forsman et al., 2015*; *Page, Muller & Vaughan, 2018*) and coral hobbyists have already put into practice: microfragmentation confers accelerated coral growth. Additionally, our analyses support the microfragmentation target of ~1 cm^2 fragments, as this size class may approach the maximum growth benefit while avoiding the increased risk of tissue loss associated with extreme variability in smaller fragment sizes (Fig. S1). Consequently, the growth produced by this technique allows coral nurseries to generate large amounts of coral biomass for outplanting onto degraded reefs in an effort to rebuild these failing ecosystems.

Tradeoffs between growth and factors that promote stress tolerance, such as constitutive immune investment, could limit the long-term success of microfragmentation-based coral restoration. This may occur if microfragmented coral in the nursery cannot withstand stressors experienced after outplanting, as all corals have an ultimate energetic budget that supports growth, metabolism, reproduction, and stress responses (*Lesser, 2013*). The limits at which a coral experiences an energetic threshold that shifts resources between growth and stress responses are not clear.

Some studies have identified positive associations between growth and coral health (*Quigley et al., 2021*; *Wright et al., 2019*) suggesting that, at least within the environmental parameters and time scales investigated, those corals could exhibit rapid growth and withstand stress. Other studies have identified tradeoffs between growth and thermal tolerance (*Cornwell et al., 2021*; *Ladd et al., 2017*) which may be linked to reduced energetics associated with thermotolerant algal symbionts (*Little, van Oppen & Willis, 2004*). Similarly, negative correlations between initial fragment size and immune activity parameters observed here could limit the ability of these fragments to restore

disease-afflicted Caribbean reefs if those differences in immune enzymes (1) persist throughout nursery rearing over longer recovery periods (*e.g.*, 12 months) and (2) actually confer increased susceptibility to disease. Our findings urgently motivate further research to address these concerns by experiments addressing the persistence of microfragmentation trade-offs over longer periods of time and experimental disease challenges. Predation by corallivores can also be a major threat to the long-term success of outplanted corals (*Aeby & Santavy, 2006*; *Gignoux-Wolfsohn, Marks & Vollmer, 2012*; *Page, Muller & Vaughan, 2018*). One study found that up to 27% of outplanted fragments were removed by fish within a single week (*Koval et al., 2020*). That same study found an additional 9% of surviving fragments showed signs of fish predation, which causes physical damage that has been linked to increased susceptibility to diseases such as White and Black Band (*Aeby & Santavy, 2006*; *Gignoux-Wolfsohn, Marks & Vollmer, 2012*; *Page, Muller & Vaughan, 2018*). The disease risk associated with predation wounding further highlights the need to ensure that coral outplants have robust immunity.

In the meantime, there is plenty of reason to have hope for microfragmented corals on Caribbean reefs. A previous report tracked out-planted microfragments over 31 months spanning two bleaching events and found no significant differences in survival between microfragments and larger corals at the same sites (*Page, Muller & Vaughan, 2018*), suggesting that microfragmented corals can withstand bleaching stress while undergoing rapid growth. Mote Marine Laboratory's Elizabeth Moore International Center for Coral Reef Research & Restoration recently reported that outplanted *O. faveolata* microfragments were able to reach sexual maturity, and successfully spawn during the annual broadcast spawning event (*Koch, Muller & Crosby, 2021*). These same fragments had survived a 2015 bleaching event, a Category four Hurricane, and an outbreak of SCTLD (*Koch, Muller & Crosby, 2021*; *Erinn Muller and Coral Restoration Team, 2021*).

Continued research into potential tradeoffs between growth and stress tolerance can inform practices to increase coral growth while limiting detrimental effects on coral health and restoration costs. For example, measuring growth rate and immune capacity throughout a longer microfragmentation recovery period (*e.g.*, 12 months) can help determine the optimal time to outplant. Other aspects of optimizing the microfragmentation procedure should be experimentally explored, documented, and standardized to accelerate the pace of coral restoration knowledge and technology. For example, a recent study found that microfragmented corals grow better on cement plugs than on more expensive ceramic plugs (*Papke et al., 2021*). It is our hope that as we expand upon our depth of knowledge, this promising protocol will continue to evolve to ensure the most promising and resilient fragments will be outplanted on degrading reefs.

Gene expression reveals biological underpinnings of rapid growth and potential immune tradeoffs

Positive associations between enzymatic activities and initial fragment size provide direct evidence for reduced constitutive immunity in microfragmented corals at the protein level. Gene expression analyses also suggest potential tradeoffs between immunity and growth.

Though they provide less direct evidence, the differentially expressed genes identified in this study present priority candidates for future research investigating mechanisms of immunity and coral growth.

Most of the variation in gene expression was explained by coral genet (ADONIS r^2: *M. cavernosa* = 0.25, *O. faveolata* = 0.35), a common finding in coral RNAseq studies (*Parkinson et al., 2015*, *2020*; *Wright et al., 2017*) that requires careful consideration when interpreting differential expression. We take a conservative approach to modeling expression by including many individuals of each genet and by including genet in the DESeq2 model. We observed subtle differences in expression that were associated with initial fragment size and growth over the recovery period. Including these two continuous factors in the model allowed us to isolate genes with linear associations with either initial size (i.e., the extent of microfragmentation) or change in buoyant weight (i.e., growth by calcification). We also conducted a binned analysis comparing expression between "small" and "big" initial size fragments and "fast" and "slow" growing fragments.

Using a continuous scale for our variables, two genes were significantly differentially expressed with respect to growth in *M. cavernosa* samples. The expression of guanylate-binding protein (GBP) was negatively associated with growth rate. GBPs have roles in mediating innate immune responses in multiple types of infections (*Praefcke, 2018*), indicating a possible tradeoff between immunity and growth rate. In *O. faveolata*, several of the 38 genes demonstrating significant negative associations with growth also play a putative role in immunity. For example, cathepsin has been found in multiple immune responses in humans, including the toll-like receptor signaling pathway (*Yadati et al., 2020*) which is also found in innate immune responses in corals (*Skutnik et al., 2020*). Integumentary mucin C.1 plays a role in microbial infection defense in mucus (*Bakshani et al., 2018*). The mucus layer is the first layer of defense in corals, and thus a critical component of a coral's tolerance to infection.

WGCNA identified groups of co-regulated genes associated with growth and immune phenotypes. Opposing correlations between module expression with growth metrics and immune parameters reflect potential gene expression tradeoffs. The three "tradeoff" modules identified by WGCNA in *M. cavernosa* are enriched with biological activities related to growth and skeletal development. A recent study identified ossification-related processes enriched in *Stylophora pistillata* exposed to reduced pH (*Scucchia et al., 2021*). That study found that acidification-resistant corals demonstrated high expression levels of cell adhesion genes, similar to the enrichment of cell junction and cell migration terms identified in the dark magenta module associated with calcification here in *M. cavernosa*. We did not observe similar enriched functions associated with growth in *O. faveolata*. Only one module associated with calcification contained any significantly enriched GO terms: light green. This module contained 69 significantly enriched GO terms with descriptions including responses to stress and reactive oxygen metabolism. The dissimilarity in enriched functions between these two coral species may reflect differences in their microfragmentation-mediated growth responses.

The associations between buoyant weight change and gene expression in *O. faveolata* offer an opportunity to reveal biological mechanisms underlying calcification.

The fragments that exhibited the most growth also had significantly higher abundances of transcripts for glutamic-rich proteins, which are key modulators of biomineralization across taxa (*Gorski, 1992*) that were recently identified in association with collagen within the skeleton of *Stylophora pistillata* (*Mummadisetti, Drake & Falkowski, 2021*). Transcripts encoding carbonic anhydrases, enzymes that catalyze the interconversion of CO_2 to bicarbonate ions driving coral calcification, exhibited the highest expression among fragments with low–intermediate growth (Fig. 5). This counterintuitive finding warrants further investigation into the mechanism of carbonic anhydrase-driven calcification, especially as previous work has shown that environmental factors can affect enzymatic activity (*Zoccola et al., 2016*). The unannotated genes identified in this study represent further opportunities to explore regulators of coral calcification.

Differentially expressed *O. faveolata* genes in the binned analysis were mostly uncharacterized, prompting further investigation of growth-related genes in this species. In the binned *M. cavernosa* analysis, a transcript with homology to tachylectin-2 was upregulated in smaller fragments. This gene product has a putative role in microbial recognition and agglutination in Japanese horseshoe crabs, *Acropora*, *Montastrea*, and *Nematostella* species (*Hayes, Eytan & Hellberg, 2010*). Several transcripts related to biomineralization were upregulated in smaller fragments, providing molecular insight into mechanisms of microfragmentation-mediated growth. The calcium ion channel polycystin-2, and other proteins in its family, have been identified as members of the skeletal organic matrix in multiple coral species (*Zaquin et al., 2021*). Both transmembrane protease serine 9-like, and coadhesin proteins, have both been linked to calcifying processes and have been found upregulated in corals with high calcification rates (*Kelley et al., 2021*; *Mummadisetti, Drake & Falkowski, 2021*; *Peled et al., 2020*).

We sampled for gene expression after the 4-month recovery period, so these results only reflect biological differences that persist long after fragmentation. This sampling time was intentional as we did not want to capture stress responses to the necessary wound inflicted during fragmentation, though future experiments may include more sampling timepoints (such as at the time of outplanting size, ~3 cm^2) to better capture the biology of wound repair and subsequent growth. We only removed tissue from the edge of each fragment to prepare the gene expression libraries, and we airbrushed the remaining edge and center tissue to measure enzymatic activities. Thus, this study only reflects gene expression at the edge of the growing fragments and cannot reveal potential difference in immune activity of edge relative to center. Given that smaller coral fragments have a higher ratio of edge:center tissue than larger fragments, differences in biological activities between these two types of tissue could underlie differences in growth and survival.

Associations between symbiont characteristics and growth

This study revealed an abundance of reads mapping to *Durusdinium* in *M. cavernosa* and *O. faveolata* (Fig. 3). Previous studies indicate that these coral species are typically dominated by *Cladocopium* in the Caribbean (*Drury et al., 2020*; *Serrano et al., 2014*; *Sturm et al., 2020*; *Warner et al., 2006*), with few exceptions (*Manzello et al., 2019*). *O. faveolata* fragments are dominated by *Durusdinium* at this particular sampling location, perhaps

because of the original environment from which the broodstock was collected or due to environmental parameters of the land-based system that promote that particular algal type. Symbiont shuffling can promote *Durusdinium* dominance in a previously *Cladocopium*-hosting coral after recovery from thermal stress (*Cunning & Baker, 2020*). Given that the suspected thermotolerance conferred by *Durusdinium* relative to *Cladocopium* may have energetic costs (*Jones & Berkelmans, 2011*) that manifest as reduced growth rates (*Cunning et al., 2015*), reef managers should continue to monitor shifts in dominant symbiont types. Comparing growth rates across corals hosting different symbiont types was not a planned goal of this research, but the observed differences in algal symbiont proportions among *M. cavernosa* samples did allow us to conduct a limited investigation. We did not find the association between growth and *Durusdinium* that others have reported, but these results are constrained by our limited sample size.

We did not find any algal symbiont genes significantly associated with coral growth. Other studies have also seen transcriptional stability within the algal symbiont (*Barshis et al., 2014*; *Davies et al., 2018*; *Leggat et al., 2011*), which may be a result of host buffering or a consequence of the unique genomic organization of the symbionts. Dinoflagellate chromosomes lack histones that regulate transcriptional dynamics in their hosts (*Rodriguez-Casariego et al., 2018*) and exist in a condensed liquid crystalline state arranged into topological domains (*Marinov et al., 2021*). Future studies could examine symbiont responses at the level of protein or metabolite rather than gene expression in order to reveal associations between algal biology and host phenotypes.

CONCLUSIONS

This study provides further evidence that the microfragmentation technique promotes faster coral growth. Future studies should continue to investigate the association between size and growth rate in corals, specifically how the surface area:edge ratio may influence growth dynamics. Enzymatic activities and specific gene expression associations with initial fragment size and growth rate reveals a possible tradeoff between microfragmentation and immunity after a 4-month recovery period. However, restoration efforts report great success with outplanted microfragments in Caribbean reefs. Future studies could investigate whether these reductions in immune activity observed in this study persist throughout the recovery period and translate to increased disease susceptibility. These gene expression patterns associated with coral calcification highlight the role of glutamic-rich proteins in biomineralization. This study identified currently unannotated genes as potentially important drivers of coral growth that represent key opportunities for further molecular characterization.

ACKNOWLEDGEMENTS

We are grateful to Erich Bartels for collecting the coral samples under FKNMS permit number FKNMS-2015-130 and to Burt D. Snover for field assistance. We thank the Texas Advanced Computing Center and Smith College Computing and Technical Services for computational resources.

ADDITIONAL INFORMATION AND DECLARATIONS

Funding

Funding was provided by a Texas State Aquarium grant awarded to Mikhail Matz.
The funders had no role in study design, data collection and analysis, decision to publish, or preparation of the manuscript.

Grant Disclosures

The following grant information was disclosed by the authors:
Texas State Aquarium grant awarded to Mikhail Matz.

Competing Interests

The authors declare that they have no competing interests.

Author Contributions

- Louis Schlecker analyzed the data, prepared figures and/or tables, authored or reviewed drafts of the paper, and approved the final draft.
- Christopher Page performed the experiments, authored or reviewed drafts of the paper, and approved the final draft.
- Mikhail Matz conceived and designed the experiments, performed the experiments, authored or reviewed drafts of the paper, and approved the final draft.
- Rachel M. Wright conceived and designed the experiments, performed the experiments, analyzed the data, prepared figures and/or tables, authored or reviewed drafts of the paper, and approved the final draft.

Field Study Permissions

The following information was supplied relating to field study approvals (*i.e.*, approving body and any reference numbers):

Field collections were collected at Florida Keys National Marine Sanctuary (FKNMS) under permit number FKNMS-2015-130

DNA Deposition

The following information was supplied regarding the deposition of DNA sequences:

The sequences are available at GenBank: PRJNA764071.

Data Availability

The following information was supplied regarding data availability:

The raw data (growth measurements, count data for both coral species M.cavernosa and O.faveolata) is available at GitHub:

https://github.com/rachelwright8/Microfrag_Growth_Immunity_TagSeq.

Supplemental Information

Supplemental information for this article can be found online at http://dx.doi.org/10.7717/peerj.13158#supplemental-information.

REFERENCES

Aeby GS, Santavy DL. 2006. Factors affecting susceptibility of the coral Montastraea faveolata to black-band disease. *Marine Ecology Progress Series* **318**:103–110 DOI 10.3354/meps318103.

Aeby GS, Ushijima B, Campbell JE, Jones S, Williams GJ, Meyer JL, Häse C, Paul VJ. 2019. Pathogenesis of a tissue loss disease affecting multiple species of corals along the Florida reef tract. *Frontiers in Marine Science* **6**:189 DOI 10.3389/fmars.2019.00678.

Altschul SF, Gish W, Miller W, Myers EW, Lipman DJ. 1990. Basic local alignment search tool. *Journal of Molecular Biology* **215(3)**:403–410 DOI 10.1016/S0022-2836(05)80360-2.

Aronson RB, Precht WF. 2001. White-band disease and the changing face of Caribbean coral reefs. In: Porter JW, ed. *The Ecology and Etiology of Newly Emerging Marine Diseases*. Netherlands: Springer, 25–38.

Bakshani CR, Morales-Garcia AL, Althaus M, Wilcox MD, Pearson JP, Bythell JC, Burgess JG. 2018. Evolutionary conservation of the antimicrobial function of mucus: a first defence against infection. *NPJ Biofilms and Microbiomes* **4(1)**:14 DOI 10.1038/s41522-018-0057-2.

Barshis DJ, Ladner JT, Oliver TA, Palumbi SR. 2014. Lineage-specific transcriptional profiles of Symbiodinium spp. unaltered by heat stress in a coral host. *Molecular Biology and Evolution* **31(6)**:1343–1352 DOI 10.1093/molbev/msu107.

Bayer T, Aranda M, Sunagawa S, Yum LK, Desalvo MK, Lindquist E, Coffroth MA, Voolstra CR, Medina M. 2012. Symbiodinium transcriptomes: genome insights into the dinoflagellate symbionts of reef-building corals. *PLOS ONE* **7(4)**:e35269 DOI 10.1371/journal.pone.0035269.

Benjamini Y, Hochberg Y. 1995. Controlling the false discovery rate: a practical and powerful approach to multiple testing. *Journal of the Royal Statistical Society* **57(1)**:289–300 DOI 10.1111/j.2517-6161.1995.tb02031.x.

Boström-Einarsson L, Babcock RC, Bayraktarov E, Ceccarelli D, Cook N, Ferse SCA, Hancock B, Harrison P, Hein M, Shaver E, Smith A, Suggett D, Stewart-Sinclair PJ, Vardi T, McLeod IM. 2020. Coral restoration-a systematic review of current methods, successes, failures and future directions. *PLOS ONE* **15(1)**:e0226631 DOI 10.1371/journal.pone.0226631.

Brown T, Rodriguez-Lanetty M. 2015. Defending against pathogens-immunological priming and its molecular basis in a sea anemone, cnidarian. *Scientific Reports* **5(1)**:17425 DOI 10.1038/srep17425.

Bruckner AW. 2016. History of coral disease research. In: Woodley CM, Downs CA, Bruckner AW, Porter JW, Galloway SB, eds. *Diseases of Coral*. First Edition. Hoboken: Wiley Blackwell, 52–84.

Bruno JF, Selig ER, Casey KS, Page CA, Willis BL, Harvell CD, Sweatman H, Melendy AM. 2007. Thermal stress and coral cover as drivers of coral disease outbreaks. *PLOS Biology* **5(6)**:e124 DOI 10.1371/journal.pbio.0050124.

Cerenius L, Lee BL, Söderhäll K. 2008. The proPO-system: pros and cons for its role in invertebrate immunity. *Trends in Immunology* **29(6)**:263–271 DOI 10.1016/j.it.2008.02.009.

Cornwell B, Armstrong K, Walker NS, Lippert M, Nestor V, Golbuu Y, Palumbi SR. 2021. Widespread variation in heat tolerance and symbiont load are associated with growth tradeoffs in the coral Acropora hyacinthus in Palau. *eLife* **10**:367 DOI 10.7554/eLife.64790.

Cramer KL, Jackson JBC, Donovan MK, Greenstein BJ, Korpanty CA, Cook GM, Pandolfi JM. 2020. Widespread loss of Caribbean acroporid corals was underway before coral bleaching and disease outbreaks. *Science Advances* **6(17)**:eaax9395 DOI 10.1126/sciadv.aax9395.

Cunning R, Baker AC. 2020. Thermotolerant coral symbionts modulate heat stress-responsive genes in their hosts. *Molecular Ecology* **29(15)**:2940–2950 DOI 10.1111/mec.15526.

Cunning R, Gillette P, Capo T, Galvez K, Baker AC. 2015. Growth tradeoffs associated with thermotolerant symbionts in the coral Pocillopora damicornis are lost in warmer oceans. *Coral Reefs* **34(1)**:155–160 DOI 10.1007/s00338-014-1216-4.

Daniels CA, Baumgarten S, Yum LK, Michell CT, Bayer T, Arif C, Roder C, Weil E, Voolstra CR. 2015. Metatranscriptome analysis of the reef-building coral *Orbicella faveolata* indicates holobiont response to coral disease. *Frontiers in Marine Science* **2(180)**:403 DOI 10.3389/fmars.2015.00062.

Davies SW, Ries JB, Marchetti A, Castillo KD. 2018. Symbiodinium functional diversity in the coral Siderastrea siderea is influenced by thermal stress and reef environment, but not ocean acidification. *Frontiers in Marine Science* **5**:17442 DOI 10.3389/fmars.2018.00150.

Denis V, Debreuil J, De Palmas S, Richard J, Guillaume MMM, Bruggemann JH. 2011. Lesion regeneration capacities in populations of the massive coral Porites lutea at Réunion Island: environmental correlates. *Marine Ecology Progress Series* **428**:105–117 DOI 10.3354/meps09060.

Dietzel A, Bode M, Connolly SR, Hughes TP. 2020. Long-term shifts in the colony size structure of coral populations along the Great Barrier Reef. *Proceedings of the Royal Society B: Biological Sciences* **287(1936)**:20201432 DOI 10.1098/rspb.2020.1432.

Dixon P. 2003. VEGAN, a package of R functions for community ecology. *Journal of Vegetation Science* **14(6)**:927–930 DOI 10.1111/j.1654-1103.2003.tb02228.x.

Drury C, Pérez Portela R, Serrano XM, Oleksiak M, Baker AC. 2020. Fine-scale structure among mesophotic populations of the great star coral Montastraea cavernosa revealed by SNP genotyping. *Ecology and Evolution* **10(12)**:6009–6019 DOI 10.1002/ece3.6340.

Edmunds PJ. 2017. Intraspecific variation in growth rate is a poor predictor of fitness for reef corals. *Ecology* **98(8)**:2191–2200 DOI 10.1002/ecy.1912.

Erinn Muller and Coral Restoration Team. 2021. Can SCTLD-susceptible species be outplanted on Florida's Coral Reef with acceptable survival rates to warrant larger-scale coral restoration efforts to commence? Retrieved from Florida Department of Environmental Protection. *Available at https://floridadep.gov/rcp/coral/documents/can-sctld-susceptible-species-be-outplanted-florida%E2%80%99s-coral-reef-acceptable*.

Forsman ZH, Page CA, Toonen RJ, Vaughan D. 2015. Growing coral larger and faster: micro-colony-fusion as a strategy for accelerating coral cover. *PeerJ* **3(1)**:e1313 DOI 10.7717/peerj.1313.

Gardner TA, Côté IM, Gill JA, Grant A, Watkinson AR. 2005. Hurricanes and caribbean coral reefs: impacts, recovery patterns, and role in long-term decline. *Ecology* **86(1)**:174–184 DOI 10.1890/04-0141.

Gignoux-Wolfsohn SA, Marks CJ, Vollmer SV. 2012. White Band Disease transmission in the threatened coral, Acropora cervicornis. *Scientific Reports* **2(1)**:804 DOI 10.1038/srep00804.

González-Santoyo I, Córdoba-Aguilar A. 2012. Phenoloxidase: a key component of the insect immune system. *Entomologia Experimentalis et Applicata* **142(1)**:1–16 DOI 10.1111/j.1570-7458.2011.01187.x.

Gorski JP. 1992. Acidic phosphoproteins from bone matrix: a structural rationalization of their role in biomineralization. *Calcified Tissue International* **50(5)**:391–396 DOI 10.1007/BF00296767.

Hadfield JD. 2010. MCMC methods for multi-response generalized linear mixed models: the MCMCglmm R package. *Journal of Statistical Software, Articles* **33(2)**:1–22 DOI 10.18637/jss.v033.i02.

Hannon GJ. 2010. FASTX-Toolkit. *Available at http://hannonlab.cshl.edu/fastx_toolkit*.

Harvell D, Jordán-Dahlgren E, Merkel S, Rosenberg E, Raymundo L, Smith G, Weil E, Willis B. 2007. Coral disease, environmental drivers, and the balance between coral and microbial associates. *Oceanography* **20(1)**:172–195 DOI 10.5670/oceanog.2007.91.

Hayes ML, Eytan RI, Hellberg ME. 2010. High amino acid diversity and positive selection at a putative coral immunity gene (tachylectin-2). *BMC Evolutionary Biology* **10(1)**:150 DOI 10.1186/1471-2148-10-150.

Hoegh-Guldberg O, Mumby PJ, Hooten AJ, Steneck RS, Greenfield P, Gomez E, Harvell CD, Sale PF, Edwards AJ, Caldeira K, Knowlton N, Eakin CM, Iglesias-Prieto R, Muthiga N, Bradbury RH, Dubi A, Hatziolos ME. 2007. Coral reefs under rapid climate change and ocean acidification. *Science* **318(5857)**:1737–1742 DOI 10.1126/science.1152509.

Jatkar AA, Brown BE, Bythell JC, Guppy R, Morris NJ, Pearson JP. 2010. Coral mucus: the properties of its constituent mucins. *Biomacromolecules* **11(4)**:883–888 DOI 10.1021/bm9012106.

Jones AM, Berkelmans R. 2011. Tradeoffs to thermal acclimation: energetics and reproduction of a reef coral with heat tolerant symbiodinium type-D. *Journal of Marine Biology* **2011(5)**:1–12 DOI 10.1155/2011/185890.

Kauffmann A, Gentleman R, Huber W. 2009. arrayQualityMetrics–a bioconductor package for quality assessment of microarray data. *Bioinformatics* **25(3)**:415–416 DOI 10.1093/bioinformatics/btn647.

Kelley ER, Sleith RS, Matz MV, Wright RM. 2021. Gene expression associated with disease resistance and long-term growth in a reef-building coral. *Royal Society Open Science* **8(4)**:210113 DOI 10.1098/rsos.210113.

Koch HR, Muller E, Crosby MP. 2021. Restored corals spawn hope for reefs worldwide. The Scientist. *Available at https://www.the-scientist.com/features/restored-corals-spawn-hope-for-reefs-worldwide-68368*.

Kolde R. 2019. pheatmap: pretty heatmaps. R package version 1.0.12. *Available at https://CRAN.R-project.org/package=pheatmap*.

Korneliussen TS, Albrechtsen A, Nielsen R. 2014. ANGSD: analysis of next generation sequencing data. *BMC Bioinformatics* **15(1)**:356 DOI 10.1186/s12859-014-0356-4.

Koval G, Rivas N, D'Alessandro M, Hesley D, Santos R, Lirman D. 2020. Fish predation hinders the success of coral restoration efforts using fragmented massive corals. *PeerJ* **8(2)**:e9978 DOI 10.7717/peerj.9978.

Ladd MC, Shantz AA, Bartels E, Burkepile DE. 2017. Thermal stress reveals a genotype-specific tradeoff between growth and tissue loss in restored Acropora cervicornis. *Marine Ecology Progress Series* **572**:129–139 DOI 10.3354/meps12169.

Ladner JT, Barshis DJ, Palumbi SR. 2012. Protein evolution in two co-occurring types of Symbiodinium: an exploration into the genetic basis of thermal tolerance in Symbiodinium clade D. *BMC Evolutionary Biology* **12(1)**:217 DOI 10.1186/1471-2148-12-217.

Landsberg JH, Kiryu Y, Peters EC, Wilson PW, Perry N, Waters Y, Maxwell KE, Huebner LK, Work TM. 2020. Stony coral tissue loss disease in Florida is associated with disruption of host-zooxanthellae physiology. *Frontiers in Marine Science* **7**:93 DOI 10.3389/fmars.2020.576013.

Langfelder P, Horvath S. 2008. WGCNA: an R package for weighted correlation network analysis. *BMC Bioinformatics* **9(1)**:559 DOI 10.1186/1471-2105-9-559.

Langmead B, Salzberg SL. 2012. Fast gapped-read alignment with Bowtie 2. *Nature Methods* **9(4)**:357–359 DOI 10.1038/nmeth.1923.

Lee EY, Lee MW, Wong GCL. 2019. Modulation of toll-like receptor signaling by antimicrobial peptides. *Seminars in Cell & Developmental Biology* **88**:173–184 DOI 10.1016/j.semcdb.2018.02.002.

Leggat W, Seneca F, Wasmund K, Ukani L, Yellowlees D, Ainsworth TD. 2011. Differential responses of the coral host and their algal symbiont to thermal stress. *PLOS ONE* **6(10)**:e26687 DOI 10.1371/journal.pone.0026687.

Lesser MP. 2013. Using energetic budgets to assess the effects of environmental stress on corals: are we measuring the right things? *Coral Reefs* **32(1)**:25–33 DOI 10.1007/s00338-012-0993-x.

Little AF, van Oppen MJH, Willis BL. 2004. Flexibility in algal endosymbioses shapes growth in reef corals. *Science* **304(5676)**:1492–1494 DOI 10.1126/science.1095733.

Love MI, Huber W, Anders S. 2014. Moderated estimation of fold change and dispersion for RNA-seq data with DESeq2. *Genome Biology* **15(12)**:550 DOI 10.1186/s13059-014-0550-8.

Lu S, Wang J, Chitsaz F, Derbyshire MK, Geer RC, Gonzales NR, Gwadz M, Hurwitz DI, Marchler GH, Song JS, Thanki N, Yamashita RA, Yang M, Zhang D, Zheng C, Lanczycki CJ, Marchler-Bauer A. 2020. CDD/SPARCLE: the conserved domain database in 2020. *Nucleic Acids Research* **48(D1)**:D265–D268 DOI 10.1093/nar/gkz991.

Manzello DP, Matz MV, Enochs IC, Valentino L, Carlton RD, Kolodziej G, Serrano X, Towle EK, Jankulak M. 2019. Role of host genetics and heat-tolerant algal symbionts in sustaining populations of the endangered coral *Orbicella faveolata* in the Florida Keys with ocean warming. *Global Change Biology* **25(3)**:1016–1031 DOI 10.1111/gcb.14545.

Marinov GK, Trevino AE, Xiang T, Kundaje A, Grossman AR, Greenleaf WJ. 2021. Transcription-dependent domain-scale three-dimensional genome organization in the dinoflagellate Breviolum minutum. *Nature Genetics* **53(5)**:613–617 DOI 10.1038/s41588-021-00848-5.

Marsh JA Jr. 1970. Primary productivity of reef-building calcareous red algae. *Ecology* **51(2)**:255–263 DOI 10.2307/1933661.

Meiling SS, Muller EM, Lasseigne D, Rossin A, Veglia AJ, MacKnight N, Dimos B, Huntley N, Correa AMS, Smith TB, Holstein DM, Mydlarz LD, Apprill A, Brandt ME. 2021. Variable species responses to experimental stony coral tissue loss disease (SCTLD) exposure. *Frontiers in Marine Science* **8**:678 DOI 10.3389/fmars.2021.670829.

Meyer E, Aglyamova GV, Matz MV. 2011. Profiling gene expression responses of coral larvae (Acropora millepora) to elevated temperature and settlement inducers using a novel RNA-Seq procedure. *Molecular Ecology* **20(17)**:3599–3616 DOI 10.1111/j.1365-294X.2011.05205.x.

Miller J, Muller E, Rogers C, Waara R, Atkinson A, Whelan KRT, Patterson M, Witcher B. 2009. Coral disease following massive bleaching in 2005 causes 60% decline in coral cover on reefs in the US Virgin Islands. *Coral Reefs* **28(4)**:925–937 DOI 10.1007/s00338-009-0531-7.

Mummadisetti MP, Drake JL, Falkowski PG. 2021. The spatial network of skeletal proteins in a stony coral. *Journal of The Royal Society Interface* **18(175)**:20200859 DOI 10.1098/rsif.2020.0859.

Mydlarz LD, Harvell CD. 2007. Peroxidase activity and inducibility in the sea fan coral exposed to a fungal pathogen. *Comparative Biochemistry and Physiology Part A: Molecular & Integrative Physiology* **146(1)**:54–62 DOI 10.1016/j.cbpa.2006.09.005.

Mydlarz LD, McGinty ES, Harvell CD. 2010. What are the physiological and immunological responses of coral to climate warming and disease? *The Journal of Experimental Biology* **213(6)**:934–945 DOI 10.1242/jeb.037580.

Mydlarz LD, Palmer CV. 2011. The presence of multiple phenoloxidases in Caribbean reef-building corals. *Comparative Biochemistry and Physiology Part A: Molecular & Integrative Physiology* **159(4)**:372–378 DOI 10.1016/j.cbpa.2011.03.029.

Neely KL, Macaulay KA, Hower EK, Dobler MA. 2020. Effectiveness of topical antibiotics in treating corals affected by Stony Coral Tissue Loss Disease. *PeerJ* **8(1)**:e9289 DOI 10.7717/peerj.9289.

Nie L, Cai S-Y, Shao J-Z, Chen J. 2018. Toll-like receptors, associated biological roles, and signaling networks in non-mammals. *Frontiers in Immunology* **9**:1523 DOI 10.3389/fimmu.2018.01523.

Page CA, Muller EM, Vaughan DE. 2018. Microfragmenting for the successful restoration of slow growing massive corals. *Ecological Engineering* **123**:86–94 DOI 10.1016/j.ecoleng.2018.08.017.

Palmer CV. 2018. Immunity and the coral crisis. *Communications Biology* **1(1)**:91 DOI 10.1038/s42003-018-0097-4.

Palmer CV, McGinty ES, Cummings DJ, Smith SM, Bartels E, Mydlarz LD. 2011. Patterns of coral ecological immunology: variation in the responses of Caribbean corals to elevated temperature and a pathogen elicitor. *The Journal of Experimental Biology* **214(24)**:4240–4249 DOI 10.1242/jeb.061267.

Palmer CV, Modi CK, Mydlarz LD. 2009. Coral fluorescent proteins as antioxidants. *PLOS ONE* **4(10)**:e7298 DOI 10.1371/journal.pone.0007298.

Palmer CV, Traylor-Knowles N. 2012. Towards an integrated network of coral immune mechanisms. *Proceedings of the Royal Society B: Biological Sciences* **279(1745)**:4106–4114 DOI 10.1098/rspb.2012.1477.

Papke E, Wallace B, Hamlyn S, Nowicki R. 2021. Differential effects of substrate type and Genet on growth of microfragments of Acropora palmata. *Frontiers in Marine Science* **8**:20400 DOI 10.3389/fmars.2021.623963.

Parkinson JE, Baker AC, Baums IB, Davies SW, Grottoli AG, Kitchen SA, Matz MV, Miller MW, Shantz AA, Kenkel CD. 2020. Molecular tools for coral reef restoration: Beyond biomarker discovery. *Conservation Letters* **13(1)**:e12687 DOI 10.1111/conl.12687.

Parkinson JE, Banaszak AT, Altman NS, LaJeunesse TC, Baums IB. 2015. Intraspecific diversity among partners drives functional variation in coral symbioses. *Scientific Reports* **5(1)**:15667 DOI 10.1038/srep15667.

Peled Y, Drake JL, Malik A, Almuly R, Lalzar M, Morgenstern D, Mass T. 2020. Optimization of skeletal protein preparation for LC-MS/MS sequencing yields additional coral skeletal proteins in Stylophora pistillata. *BMC Materials* **2(1)**:8 DOI 10.1186/s42833-020-00014-x.

Prada C, Hanna B, Budd AF, Woodley CM, Schmutz J, Grimwood J, Iglesias-Prieto R, Pandolfi JM, Levitan D, Johnson KG, Knowlton N, Kitano H, DeGiorgio M, Medina M. 2016. Empty niches after extinctions increase population sizes of modern corals. *Current Biology* **26**:3190–3194 DOI 10.1016/j.cub.2016.09.039.

Praefcke GJK. 2018. Regulation of innate immune functions by guanylate-binding proteins. *International Journal of Medical Microbiology* **308(1)**:237–245 DOI 10.1016/j.ijmm.2017.10.013.

Precht WF, Gintert BE, Robbart ML, Fura R, van Woesik R. 2016. Unprecedented disease-related coral mortality in southeastern florida. *Scientific Reports* **6(1)**:31374 DOI 10.1038/srep31374.

Quigley KM, Marzonie M, Ramsby B, Abrego D, Milton G, van Oppen MJH, Bay LK. 2021. Variability in fitness trade-offs amongst coral juveniles with mixed genetic backgrounds held in the wild. *Frontiers in Marine Science* **8**:3532 DOI 10.3389/fmars.2021.636177.

Randall CJ, Jordan-Garza AG, Muller EM, van Woesik R. 2014. Relationships between the history of thermal stress and the relative risk of diseases of Caribbean corals. *Ecology* **95(7)**:1981–1994 DOI 10.1890/13-0774.1.

Reaka-Kudla ML. 2001. Known and unknown biodiversity, risk of extinction and conservation strategy in the sea. In: Bendell-Young L, Gallaugher P, eds. *Waters in Peril*. US: Springer, 19–33.

ReFuGe 2020 Consortium. 2015. The ReFuGe 2020 Consortium—using "omics" approaches to explore the adaptability and resilience of coral holobionts to environmental change. *Frontiers in Marine Science* **2**:e00068 DOI 10.3389/fmars.2015.00068.

Rodriguez-Casariego JA, Ladd MC, Shantz AA, Lopes C, Cheema MS, Kim B, Roberts SB, Fourqurean JW, Ausio J, Burkepile DE, Eirin-Lopez JM. 2018. Coral epigenetic responses to nutrient stress: Histone H2A.X phosphorylation dynamics and DNA methylation in the staghorn coral Acropora cervicornis. *Ecology and Evolution* **8(23)**:12193–12207 DOI 10.1002/ece3.4678.

Rosales SM, Clark AS, Huebner LK, Ruzicka RR, Muller EM. 2020. Rhodobacterales and rhizobiales are associated with stony coral tissue loss disease and its suspected sources of transmission. *Frontiers in Microbiology* **11**:681 DOI 10.3389/fmicb.2020.00681.

RStudio Team. 2020. RStudio: integrated development environment for R. RStudio, PBC, Boston, MA. *Available at http://www.rstudio.com/*.

Sadd BM, Siva-Jothy MT. 2006. Self-harm caused by an insect's innate immunity. *Proceedings of the Royal Society B: Biological Sciences* **273(1600)**:2571–2574 DOI 10.1098/rspb.2006.3574.

Schneider CA, Rasband WS, Eliceiri KW. 2012. NIH Image to ImageJ: 25 years of image analysis. *Nature Methods* **9(7)**:671–675 DOI 10.1038/nmeth.2089.

Scucchia F, Malik A, Putnam HM, Mass T. 2021. Genetic and physiological traits conferring tolerance to ocean acidification in mesophotic corals. *Global Change Biology* **27(20)**:5276–5294 DOI 10.1111/gcb.15812.

Serrano X, Baums IB, O'Reilly K, Smith TB, Jones RJ, Shearer TL, Nunes FLD, Baker AC. 2014. Geographic differences in vertical connectivity in the Caribbean coral Montastraea cavernosa despite high levels of horizontal connectivity at shallow depths. *Molecular Ecology* **23(17)**:4226–4240 DOI 10.1111/mec.12861.

Shilling EN, Combs IR, Voss JD. 2021. Assessing the effectiveness of two intervention methods for stony coral tissue loss disease on Montastraea cavernosa. *Scientific Reports* **11(1)**:8566 DOI 10.1038/s41598-021-86926-4.

Shoguchi E, Beedessee G, Hisata K, Tada I, Narisoko H, Satoh N, Kawachi M, Shinzato C. 2021. A new dinoflagellate genome illuminates a conserved gene cluster involved in sunscreen biosynthesis. *Genome Biology and Evolution* **13(2)**:3532 DOI 10.1093/gbe/evaa235.

Skutnik JE, Otieno S, Khoo SK, Strychar KB. 2020. Examining the effect of heat stress on montastraea cavernosa (Linnaeus 1767) from a mesophotic coral ecosystem (MCE). *Water* **12(5)**:1303 DOI 10.3390/w12051303.

Spencer Davies P. 1989. Short-term growth measurements of corals using an accurate buoyant weighing technique. *Marine Biology* **101(3)**:389–395 DOI 10.1007/BF00428135.

Sturm AB, Eckert RJ, Méndez JG, González-Díaz P, Voss JD. 2020. Population genetic structure of the great star coral, Montastraea cavernosa, across the Cuban archipelago with comparisons between microsatellite and SNP markers. *Scientific Reports* **10(1)**:15432 DOI 10.1038/s41598-020-72112-5.

Sully S, Burkepile DE, Donovan MK, Hodgson G, van Woesik R. 2019. A global analysis of coral bleaching over the past two decades. *Nature Communications* **10(1)**:1264 DOI 10.1038/s41467-019-09238-2.

Traylor-Knowles N, Connelly MT, Young BD, Eaton K, Muller EM, Paul VJ, Ushijima B, DeMerlis A, Drown MK, Goncalves A, Kron N, Snyder GA, Martin C, Rodriguez K. 2021. Gene expression response to stony coral tissue loss disease transmission in M. cavernosa and O. faveolata From Florida. *Frontiers in Marine Science* **8**:91 DOI 10.3389/fmars.2021.681563.

Vidal-Dupiol J, Ladrière O, Destoumieux-Garzón D, Sautière P-E, Meistertzheim A-L, Tambutté E, Tambutté S, Duval D, Fouré L, Adjeroud M, Mitta G. 2011. Innate immune responses of a scleractinian coral to vibriosis. *The Journal of Biological Chemistry* **286(25)**:22688–22698 DOI 10.1074/jbc.M110.216358.

Warner ME, LaJeunesse TC, Robison JD, Thur RM. 2006. The ecological distribution and comparative photobiology of symbiotic dinoflagellates from reef corals in Belize: potential implications for coral bleaching. *Limnology and Oceanography* **51(4)**:1887–1897 DOI 10.4319/lo.2006.51.4.1887.

Weil E, Hernández-Delgado EA, Gonzalez M, Williams S, Suleimán-Ramos S, Figuerola M, Metz-Estrella T. 2019. Spread of the new coral disease SCTLD into the Caribbean: implications for Puerto Rico. *Reef Encounter* **34**:38–43.

Williams LM, Fuess LE, Brennan JJ, Mansfield KM, Salas-Rodriguez E, Welsh J, Awtry J, Banic S, Chacko C, Chezian A, Dowers D, Estrada F, Hsieh Y-H, Kang J, Li W, Malchiodi Z, Malinowski J, Matuszak S, McTigue T IV, Mueller D, Nguyen B, Nguyen M, Nguyen P, Nguyen S, Njoku N, Patel K, Pellegrini W, Pliakas T, Qadir D, Ryan E, Schiffer A, Thiel A, Yunes SA, Spilios KE, Pinzón CJH, Mydlarz LD, Gilmore TD. 2018. A conserved Toll-like receptor-to-NF-κB signaling pathway in the endangered coral *Orbicella faveolata*. *Developmental and Comparative Immunology* **79**:128–136 DOI 10.1016/j.dci.2017.10.016.

Wright RM, Aglyamova GV, Meyer E, Matz MV. 2015. Gene expression associated with white syndromes in a reef building coral, Acropora hyacinthus. *BMC Genomics* **16(1)**:371 DOI 10.1186/s12864-015-1540-2.

Wright RM, Kenkel CD, Dunn CE, Shilling EN, Bay LK, Matz MV. 2017. Intraspecific differences in molecular stress responses and coral pathobiome contribute to mortality under bacterial challenge in Acropora millepora. *Scientific Reports* **7(1)**:2609 DOI 10.1038/s41598-017-02685-1.

Wright RM, Mera H, Kenkel CD, Nayfa M, Bay LK, Matz MV. 2019. Positive genetic associations among fitness traits support evolvability of a reef-building coral under multiple stressors. *Global Change Biology* **25(10)**:3294–3304 DOI 10.1111/gcb.14764.

Yadati T, Houben T, Bitorina A, Shiri-Sverdlov R. 2020. The ins and outs of cathepsins: physiological function and role in disease management. *Cells* **9(7)**:1679 DOI 10.3390/cells9071679.

Zaquin T, Malik A, Drake JL, Putnam HM, Mass T. 2021. Evolution of protein-mediated biomineralization in scleractinian corals. *Frontiers in Genetics* **12**:618517 DOI 10.3389/fgene.2021.618517.

Zoccola D, Innocenti A, Bertucci A, Tambutté E, Supuran CT, Tambutté S. 2016. Coral carbonic anhydrases: regulation by ocean acidification. *Marine Drugs* **14(6)**:109 DOI 10.3390/md14060109.